Universiteit
Leiden
The Netherlands

Computational electrocatalysis: methods and fundamental applications on CO2 reduction and formic acid oxidation

Granda Marulanda, L.P.

Citation
Granda Marulanda, L. P. (2021, October 19). *Computational electrocatalysis: methods and fundamental applications on CO2 reduction and formic acid oxidation*. Retrieved from https://hdl.handle.net/1887/3217519

Version:	Publisher's Version
License:	Licence agreement concerning inclusion of doctoral thesis in the Institutional Repository of the University of Leiden
Downloaded from:	https://hdl.handle.net/1887/3217519

Note: To cite this publication please use the final published version (if applicable).

Park Güell
Barcelona, Catalonia, Spain

2 Influence of Van der Waals interactions on the solvation energies of adsorbates at Pt-based electrocatalysts

Solvation can significantly modify the adsorption energy of species at surfaces, thereby influencing the performance of electrocatalysts and liquid-phase catalysts. Thus, it is important to understand adsorbate solvation at the nanoscale. Here we evaluate the effect of van der Waals (vdW) interactions described by different approaches on the solvation energy of *OH adsorbed on near-surface alloys (NSAs) of Pt. Our results show that the studied functionals can be divided into two groups, each with rather similar average *OH solvation energies: (1) PBE and PW91; and (2) vdW functionals, RPBE, PBE-D3 and RPBE-D3. On average, *OH solvation energies are less negative by ~0.14 eV in group (2) compared to (1), and the values for a given alloy can be extrapolated from one functional to another within the same group. Depending on the desired level of accuracy, these concrete observations and our tabulated values can be used to rapidly incorporate solvation into models for electrocatalysis and liquid-phase catalysis.

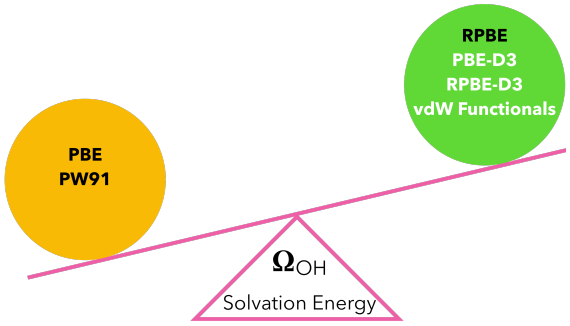

This chapter is based on Granda-Marulanda, L. P.; Builes, S.; Koper, M. T. M.; Calle-Vallejo, F. Influence of Van Der Waals Interactions on the Solvation Energies of Adsorbates at Pt-Based Electrocatalysts. ChemPhysChem 2019, 20 (22), 2968–2972

2.1 Introduction

The solvation of adsorbates is becoming a topic of great interest in computational electrocatalysis in view of the current search for more realistic representations of electrode-electrolyte interfaces. Numerous recent experimental works show that solvent and/or electrolyte effects change the activity and selectivity of electrocatalysts for important reactions such as oxygen reduction,[1,2] hydrogen evolution,[3,4] CO_2 reduction,[5,6] and CO reduction.[7,8] In addition, computational works show that solvation and/or cation co-adsorption modify the adsorption energies of reaction intermediates,[9–13] which may not only lead to changes in reaction pathways[14] but also to considerable differences in the calculated activity of electrocatalysts.[10,15]In computational electrocatalysis adsorbate-solvent and adsorbate-electrolyte interactions at the interface can be evaluated implicitly (where the solvent is modelled as a continuum with certain dielectric constant),[13,16–25] explicitly,[26–33] or through combinations of the two.[34,35] Furthermore, less expensive explicit solvation models, sometimes referred as "micro-solvation" or near-surface solvation[36–38] have been tailored to save computational resources by using a small number of explicit water molecules to stabilize a given adsorbate.

The role of vdW forces on water clustering, water-metal interactions, and liquid water has been explored by using functionals that account for vdW interactions.[39–43] In general, dispersion-corrected functionals or those incorporating vdW forces self-consistently tend to increase the adsorption energy of water on metal surfaces. However, the majority of computational electrocatalysis studies carried out within the framework of Density Functional theory (DFT) use common exchange-correlation (xc) functionals that do not account for van der Waals (vdW) interactions. Importantly, those might be necessary for an accurate description of water-water, water-electrode and water-adsorbate interactions.

This ***Chapter*** presents a study of the role of vdW interactions on the solvation energy of hydroxyl (*OH) adsorbed on near-surface alloys (NSAs) of Pt and late transition metals. Those versatile alloys are salient model catalysts for a variety of electrocatalytic reactions.[44–47] We observe that: (1) the predictions of *OH solvation at Pt NSAs are comparable for PBE and PW91. (2) The predictions of *OH solvation at Pt NSAs are comparable among RPBE, vdW functionals and GGAs with dispersion corrections. (3) The *OH solvation energies decrease on average by ~0.14 eV from functionals in (2) with respect to those in (1).

2.2 Computational details

The DFT calculations were carried out using the PAW[48] method in the Vienna Ab initio Simulation Package[49]. We simulated √3×√3 R30º slabs of Pt(111) NSAs with 1 monolayer (ML) of late transition metal atoms in the subsurface (see Figure 2.1) and: (I) 1/3 ML *OH in vacuum, (II) 1/3 ML *OH + 1/3 ML *H_2O, and (III) 2/3 ML *H_2O. The subsurface metals were Co, Ni, Cu, Rh, Pd, Ag, Ir, Pt and Au. The slabs contained four atomic layers: the two uppermost layers and the adsorbates were fully relaxed, while the two bottommost layers were fixed at the converged

interatomic distances of bulk Pt calculated for each exchange-correlation functional. All of the calculated lattice constants appear in Table A8 in the SI. H_2 and H_2O were simulated in cubic boxes of 3375 $Å^3$. In all simulations, we used 0.01 eV $Å^{-1}$ as convergence criterion for the maximal forces on the atoms, and a plane-wave cutoff of 450 eV.

The k-point samplings were 8×8×1 for the slabs and 1×1×1 for H_2 and H_2O. For the slabs, ~15 Å of vacuum and dipole corrections in the z direction were used to avoid artificial electrostatic interactions between periodic images. The Methfessel-Paxton method[50] was employed to smear the Fermi level of the slabs with k_BT = 0.2 eV, whereas Gaussian smearing was used for H_2 and H_2O with k_BT = 0.001 eV. In both cases, all energies were extrapolated to 0 K. We used the computational hydrogen electrode to assess the energetics of solvated protons and electrons.[51] As a first approximation, we made spin-restricted calculations for Ni- and Co-containing NSAs. The free energies were evaluated as: $G = E_{DFT} + ZPE - TS$. The zero-point energy corrections (ZPE) of gases and adsorbates, as well as the adsorbates' vibrational entropies were calculated within the harmonic-oscillator approximation. The $TS_{total}^{298.15K}$ corrections for H_2(g) and H_2O(l) are 0.40 and 0.67 eV.[51] We used the following exchange-correlation functionals: PW91,[52] PBE,[53] RPBE[54]; functionals with semi-empirical corrections, PBE-D3 and RPBE-D3, using the DFT-D3 method[55]; a functional that evaluates vdW interactions with an optimized version of vdW-DF method,[56] namely optPBE[43]; and the BEEF-vdW functional.[57] Specific energetic and geometric data related to this study appear in the Appeendix A, Figure A3 and Tables A1-A8.

2.3 Results and discussion

Following previous works,[11,37] to obtain the free energy of solvation, (Ω_{OH}), for *OH on the √3×√3 R30° slab, we determined: (i) the free energy of formation of 1/3 ML *OH coadsorbed with 1/3 ML *H_2O with respect to an ice-like water bilayer with 2/3 ML *H_2O ($\Delta G_{OH}^{H_2O}$),[41,58,59] as shown in Eq. 2.1 and in Figure 2.1a. (ii) The free energy of formation of 1/3ML *OH in vacuum with respect to H_2O(l) (ΔG_{OH}^{vac}) using Eq. 2.2, as depicted in Figure 1b.

$$2 * H_2O \rightarrow *OH + * H_2O + H^+ + e^- \qquad 2.1$$

$$* + H_2O(l) \rightarrow *OH + H^+ + e^- \qquad 2.2$$

where * represents an active site at the surface of the NSAs. Recent works have shown that three *H_2O molecules are required to solvate *OH, as the O atom in *OH can make two hydrogen bonds with surrounding water molecules and the H atom can make one.[37] This is also the case for the periodic water bilayers considered here, as shown in Figure 2.1a. The difference between Eq. 2.1 and Eq. 2.2 gives the solvation contribution to the free energy of adsorption (Ω_{OH}):

$$\Omega_{OH} = \Delta G_{OH}^{H_2O} - \Delta G_{OH}^{vac} \quad 2.3$$

Once Ω_{OH} is known, it can be added to other adsorption energies calculated in vacuum ($\Delta G_{OH}^{vac\#}$) to obtain a first assessment of the adsorption energies in solution ($\Delta G_{OH}^{H_2O\#}$), which are usually burdensome to calculate:[37]

$$\Delta G_{OH}^{H_2O\#} \approx \Delta G_{OH}^{vac\#} + \Omega_{OH} \quad 2.4$$

where the superscript # indicates an extrapolation, hence the approximate sign. Previous works concluded that one can extrapolate Ω_{OH} from one facet to another of a given material,[37] but that it is not advisable to do so among different materials.[9–11] In the following, we will analyze whether such extrapolations are possible when Ω_{OH} is calculated with a different functional than ΔG_{OH}^{vac}. This is a common situation when using tabulated results from previous works.

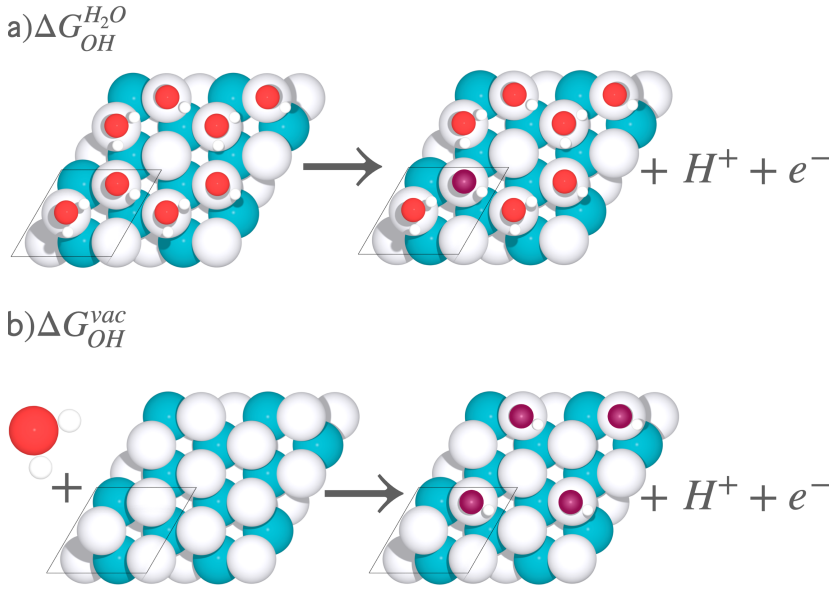

FIGURE 2.1
Schematics of Eq. 2.1 and Eq. 2.2 for the free energies of formation of *OH on Pt NSAs. (a) 1/3 ML *OH coadsorbed with 1/3 ML *H_2O (right side) using as a reference a water bilayer (left side) with one water molecule in the flat configuration and the other one with a hydrogen pointing towards the surface. (b) 1/3 ML *OH in vacuum (right side) using liquid water as a reference (left side). In both cases the slabs are 2×2 repetitions of a (111) √3×√3 R30° supercell as defined by the parallelogram. Each layer in the slab contains 3 metal atoms. Pt: gray, subsurface metal: turquoise, O in H_2O: red, O in OH: purple, H: white. A top and side view of the water adlayer can be seen in Figure A3.

Table 2.1 provides the solvation corrections obtained for *OH with different functionals for nine different Pt NSAs. We have split the functionals into two groups: group 1, formed by PW91 and PBE, and group 2, formed by RPBE, PBE-D3, RPBE-D3, optPBE and BEEF-vdW.

In the following, we explain the creation of two groups and the presence of RPBE (a GGA) in group 2 (with vdW and dispersion-corrected functionals) instead of group 1 (other GGAs).

Although PBE and PW91 are not entirely equivalent,[60] they do provide similar values for properties such as atomization energies and lattice constants. For example, for the latter property, PW91 gave 3.99 Å and PBE 3.98 Å (see Table A8). Therefore, for adsorption free energies it is expected that the results do not differ significantly. Indeed, we found for Ω_{OH} that the average values for PBE/PW91 are similar (see Table 2.1).

In general, RPBE and PBE/PW91 give different results for properties such as atomization energies for molecules and equilibrium cell volumes for solids.[61] It has been shown that PBE/PW91 over-bind adsorbates to surfaces with respect to experiments, while RPBE under-binds them,[62] which is presumably connected to RPBE's severe underestimation of surface energies.[63]

Here we observe something similar: the *OH solvation corrections for NSAs, which are the difference between the adsorption energies of *OH in solution and in vacuum, Eq. 2.3, are on average ~0.15 eV more negative for PBE compared to RPBE (see Table 2.1). This is because on average, ΔG_{OH}^{vac} is 0.11 eV weaker for RPBE vs PBE, whereas $\Delta G_{OH}^{H_2O}$ is weaker by 0.26 eV (see Tables A2 and A3). We note that the trends in Ω_{OH}, $\Delta G_{OH}^{H_2O}$, and ΔG_{OH}^{vac} as a function of the number of valence electrons (see Table 2.1 and Figure A2) are similar for PBE, PW91 and RPBE.

The less negative average solvation energy with respect to PBE/PW91 is also observed for functionals incorporating vdW interactions and dispersion corrections. This is because the adsorbate-metal interactions are more strongly enhanced for ΔG_{OH}^{vac} compared to $\Delta G_{OH}^{H_2O}$, in view of the presence of H_2O in the latter.[39] On average, ΔG_{OH}^{vac} is strengthened by 0.17 eV for PBE-D3 with respect to PBE, whereas $\Delta G_{OH}^{H_2O}$ is strengthened only by 0.02 eV (see Tables A2 and A3). We attribute this to the enhanced water-substrate interactions provided by dispersion corrections: the average adsorption energy of the water bilayer is made more negative by 0.22 eV for PBE-D3 with respect to PBE (see Table A4). In fact, it is well known that dispersion corrections increase the binding energy of water adlayers on substrates,[43] which according to Eq. 2.1 and Eq. 2.3 makes the solvation energies less negative.

Altogether, in group 1 we have PBE and PW91, which are over-binding GGAs, while in group 2 we have under-binding GGAs such as RPBE together with vdW functionals and dispersion-corrected functionals. The average solvation energy for the functionals in group 1 is -0.55 eV, while it is -0.40 eV for the functionals in group 2. We emphasize that the division of functionals in groups 1 and 2 is based merely on the results, and a rigorous classification would require data from additional functionals and adsorbates.

Regarding the safe use of Eq. 2.4, there are two important points to be considered: first, for a given functional, the variations among the different alloys are large. The standard deviation for the alloys in groups 1 and 2 is 0.09 and 0.08 eV, respectively. In line with previous works focused on PBE only,[11] our conclusion is that it is unadvisable to use a single solvation correction for all

alloys. Second, for a given alloy one can combine among functionals from either group 1 or group 2, but not between groups. The mean of the standard deviations for the alloys are 0.03 and 0.02 eV for groups 1 and 2, respectively. Essentially, applying PBE-calculated solvation energies to PW91's adsorption energies in vacuum (and vice versa) is possible using Eq. 2.4, as the solvation corrections are similar for both functionals. Ω_{OH} values can also be extrapolated from one functional to another within group 2. However, it is preferable not to extrapolate values of group 1 to group 2 and vice versa, as the differences are on average ~0.15 eV. For instance, the design principle for oxygen reduction catalysts states that optimal catalysts should bind around 0.10 – 0.15 eV weaker than Pt(111), $\Delta G_{OH} - \Delta G_{OH}^{Pt(111)} \approx 0.1 - 0.15$ eV,[11,64,65] so it is advisable to avoid intergroup extrapolations. Table 2.1 provides the average values (avg1/avg2) and standard deviations (stdev1/stdev2) for each alloy in each group. Figure A2 shows the energy trends for the two groups. The average and standard deviation for a given alloy across all functionals appear in Table A1.

TABLE 2.1

Free energies of solvation (Ω_{OH}) in eV for 1/3 ML *OH coadsorbed with 1/3 ML *H_2O within a water bilayer using different functionals. avg1 and avg2 are the averages of the solvation energies for group 1 functionals (PBE, PW91) and group 2 functionals (RPBE, vdW functionals: optPBE and BEEF-vdW, and with dispersion corrections: PBE-D3 and RPBE-D3) across the same metal. Stdev1/2 are the corresponding standard deviations of avg1/avg2. MAX and MIN are the maximal and minimal values in the dataset across the same functional. Range is the difference between MAX and MIN.

METAL	PW91	PBE	RPBE	PBE–D3	RPBE–D3	opt-PBE	BEEF–vdW	avg1	avg2	stdev1	stdev2
Co	-0.60	-0.69	-0.50	-0.45	-	-0.52	-0.48	-0.64	-0.49	0.07	0.03
Rh	-0.61	-0.61	-0.45	-0.47	-0.48	-0.47	-0.39	-0.61	-0.45	0.00	0.04
Ir	-0.63	-0.63	-0.43	-0.50	-0.50	-0.49	-0.43	-0.63	-0.47	0.00	0.04
Ni	-0.53	-0.52	-0.40	-0.43	-0.45	-0.43	-0.44	-0.53	-0.43	0.01	0.02
Pd	-0.56	-0.56	-0.36	-0.40	-0.41	-0.40	-0.39	-0.56	-0.39	0.00	0.02
Pt	-0.62	-0.62	-0.50	-0.45	-0.57	-0.45	-0.44	-0.62	-0.48	0.00	0.05
Cu	-0.50	-0.42	-0.32	-0.31	-0.27	-0.29	-0.28	-0.46	-0.29	0.06	0.02
Ag	-0.40	-0.38	-0.26	-0.25	-0.27	-0.25	-0.27	-0.39	-0.26	0.02	0.01
Au	-0.49	-0.50	-0.35	-0.35	-0.46	-0.35	-0.33	-0.49	-0.37	0.01	0.05
mean	-0.55	-0.55	-0.39	-0.40	-0.43	-0.41	-0.38				
stdev	0.08	0.10	0.08	0.08	0.11	0.09	0.07				
MAX	-0.40	-0.38	-0.26	-0.25	-0.27	-0.25	-0.27				
MIN	-0.63	-0.69	-0.50	-0.50	-0.57	-0.52	-0.48				
range	0.23	0.32	0.24	0.25	0.30	0.27	0.21				

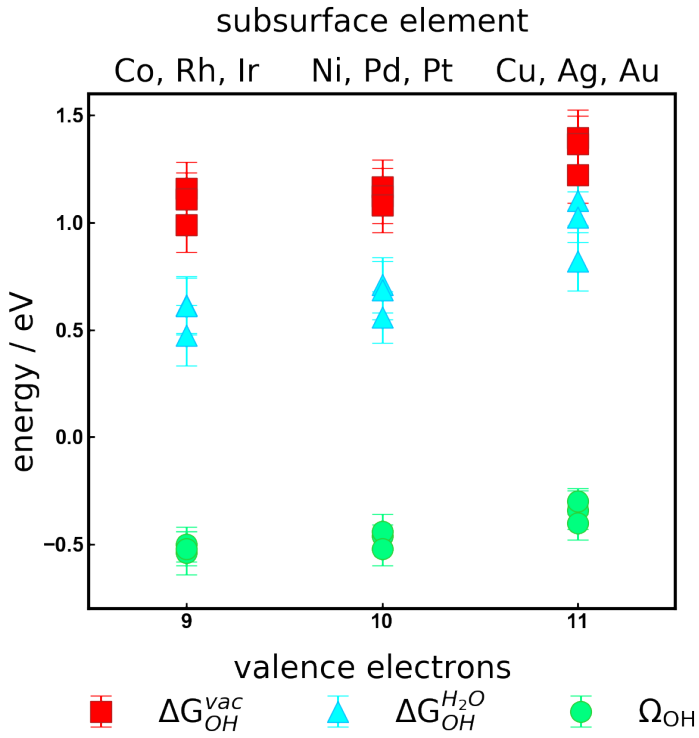

FIGURE 2.2

Adsorption energies of 1/3 ML *OH in vacuum (red, ΔG_{OH}^{vac}), within the water bilayer (blue, $\Delta G_{OH}^{H_2O}$), and in the solvation energy (green, Ω_{OH}), as a function of the number of valence electrons of the subsurface metal atom in the Pt NSAs. The error bars cover the energy range spanned by the different functionals analyzed. The correlation between the number of valence electrons and the d-band centers of the Pt skins is provided in Figure A1.

Figure 2.2 summarizes the trends in adsorption energies in vacuum and in solution together with the *OH solvation energies, as a function of the number of electrons of the metal in the Pt NSAs (see also Figure A1). The data points are the average values for each NSA considering all functionals (avg0) in Tables A2, A3, and A1 for ΔG_{OH}^{vac}, $\Delta G_{OH}^{H_2O}$, and Ω_{OH}, respectively. The error bars correspond to the standard deviation across the metals (stdev0) in Tables A2, A3 and A1, respectively. Importantly, the size of the error bars decreases for Ω_{OH} with respect to ΔG_{OH}^{vac} and $\Delta G_{OH}^{H_2O}$. This shows that: (i) the number of valence electrons of the components can be used to predict solvation corrections, in line with previous works on adsorption-energy trends;[11,66–68] and (ii) because Ω_{OH} results from the difference of ΔG_{OH}^{vac} and $\Delta G_{OH}^{H_2O}$ (Eq. 2.3), its actual values are considerably less functional-dependent than those of the original adsorption energies.

2.4 Conclusions

Using *OH adsorbed on Pt near-surface alloys with transition metals as a case study, we showed that accounting for long-range interactions generally results in a decrease of the strength of solvation contributions to the adsorption energies with respect to GGAs. The decrease is on average ~0.14 eV and is due to the enhancement of water-metal interactions when including long-range interactions. The solvation energies of *OH calculated with PBE are similar to those of PW91 but differ ~0.15 eV from those of RPBE. Solvation energies calculated with RPBE, vdW functionals (optPBE and BEEF-vdW) and dispersion-corrected GGA functionals (PBE-D3 and RPBE-D3) are generally rather similar. Furthermore, solvation corrections can be predicted based on the number of valence electrons of the subsurface metal in the alloy. Depending on the desired level of accuracy, these guidelines can be used to decide whether specific solvation energies need to be calculated or if average values suffice, which can help in making more efficient electrocatalysis and liquid-phase catalysis models.

2.5 References

(1) Garlyyev, B.; Xue, S.; Pohl, M. D.; Reinisch, D.; Bandarenka, A. S. Oxygen Electroreduction at High-Index Pt Electrodes in Alkaline Electrolytes: A Decisive Role of the Alkali Metal Cations. *ACS Omega* **2018**, *3* (11), 15325–15331.

(2) Zhao, X.; Gunji, T.; Kaneko, T.; Yoshida, Y.; Takao, S.; Higashi, K.; Uruga, T.; He, W.; Liu, J.; Zou, Z. An Integrated Single-Electrode Method Reveals the Template Roles of Atomic Steps: Disturb Interfacial Water Networks and Thus Affect the Reactivity of Electrocatalysts. *J. Am. Chem. Soc.* **2019**.

(3) Xue, S.; Garlyyev, B.; Watzele, S.; Liang, Y.; Fichtner, J.; Pohl, M. D.; Bandarenka, A. S. Influence of Alkali Metal Cations on the Hydrogen Evolution Reaction Activity of Pt, Ir, Au, and Ag Electrodes in Alkaline Electrolytes. *ChemElectroChem* **2018**, *5* (17), 2326–2329.

(4) Ledezma-Yanez, I.; Wallace, W. D. Z.; Sebastián-Pascual, P.; Climent, V.; Feliu, J. M.; Koper, M. T. M. Interfacial Water Reorganization as a PH-Dependent Descriptor of the Hydrogen Evolution Rate on Platinum Electrodes. *Nature Energy* **2017**, *2* (4), nenergy201731.

(5) Varela, A. S.; Ju, W.; Reier, T.; Strasser, P. Tuning the Catalytic Activity and Selectivity of Cu for CO2 Electroreduction in the Presence of Halides. *ACS Catal.* **2016**, *6* (4), 2136–2144.

(6) Singh, M. R.; Kwon, Y.; Lum, Y.; Ager, J. W.; Bell, A. T. Hydrolysis of Electrolyte Cations Enhances the Electrochemical Reduction of CO2 over Ag and Cu. *J. Am. Chem. Soc.* **2016**, *138* (39), 13006–13012.

(7) Murata, A.; Hori, Y. Product Selectivity Affected by Cationic Species in Electrochemical Reduction of CO2 and CO at a Cu Electrode. *Bulletin of The Chemical Society of Japan - BULL CHEM SOC JPN* **1991**, *64*, 123–127.

(8) Pérez-Gallent, E.; Marcandalli, G.; Figueiredo, M. C.; Calle-Vallejo, F.; Koper, M. T. M. Structure- and Potential-Dependent Cation Effects on CO Reduction at Copper Single-Crystal Electrodes. *J. Am. Chem. Soc.* **2017**, *139* (45), 16412–16419.
(9) Tripkovic, V. Thermodynamic Assessment of the Oxygen Reduction Activity in Aqueous Solutions. *Phys. Chem. Chem. Phys.* **2017**, *19* (43), 29381–29388.
(10) Calle-Vallejo, F.; Krabbe, A.; M. García-Lastra, J. How Covalence Breaks Adsorption-Energy Scaling Relations and Solvation Restores Them. *Chemical Science* **2017**, *8* (1), 124–130.
(11) He, Z.-D.; Hanselman, S.; Chen, Y.-X.; Koper, M. T. M.; Calle-Vallejo, F. Importance of Solvation for the Accurate Prediction of Oxygen Reduction Activities of Pt-Based Electrocatalysts. *J. Phys. Chem. Lett.* **2017**, *8* (10), 2243–2246.
(12) Gray, C. M.; Saravanan, K.; Wang, G.; Keith, J. A. Quantifying Solvation Energies at Solid/Liquid Interfaces Using Continuum Solvation Methods. *Molecular Simulation* **2017**, *43* (5–6), 420–427.
(13) Ludwig, T.; Gauthier, J. A.; Brown, K. S.; Ringe, S.; Nørskov, J. K.; Chan, K. Solvent–Adsorbate Interactions and Adsorbate-Specific Solvent Structure in Carbon Dioxide Reduction on a Stepped Cu Surface. *J. Phys. Chem. C* **2019**, *123* (10), 5999–6009.
(14) Calle-Vallejo, F.; Koper, M. T. M. Accounting for Bifurcating Pathways in the Screening for CO2 Reduction Catalysts. *ACS Catal.* **2017**, *7* (10), 7346–7351.
(15) Briquet, L. G. V.; Sarwar, M.; Mugo, J.; Jones, G.; Calle-Vallejo, F. A New Type of Scaling Relations to Assess the Accuracy of Computational Predictions of Catalytic Activities Applied to the Oxygen Evolution Reaction. *ChemCatChem* **2017**, *9* (7), 1261–1268.
(16) Letchworth-Weaver, K.; Arias, T. A. Joint Density-Functional Theory of the Electrode-Electrolyte Interface: Application to Fixed Electrode Potentials, Interfacial Capacitances, and Potentials of Zero Charge. *Physical Review B* **2012**, *86* (7).
(17) Schwarz, K. A.; Sundararaman, R.; Moffat, T. P.; Allison, T. C. Formic Acid Oxidation on Platinum: A Simple Mechanistic Study. *Phys. Chem. Chem. Phys.* **2015**, *17* (32), 20805–20813.
(18) Sundararaman, R.; Schwarz, K. Evaluating Continuum Solvation Models for the Electrode-Electrolyte Interface: Challenges and Strategies for Improvement. *The Journal of Chemical Physics* **2017**, *146* (8), 084111.
(19) Mathew, K.; Sundararaman, R.; Letchworth-Weaver, K.; Arias, T. A.; Hennig, R. G. Implicit Solvation Model for Density-Functional Study of Nanocrystal Surfaces and Reaction Pathways. *J. Chem. Phys.* **2014**, *140* (8), 084106.
(20) Mathew, K.; Hennig, R. G. Implicit Self-Consistent Description of Electrolyte in Plane-Wave Density-Functional Theory. *arXiv:1601.03346 [cond-mat]* **2016**.
(21) Garcia-Ratés, M.; López, N. Multigrid-Based Methodology for Implicit Solvation Models in Periodic DFT. *J. Chem. Theory Comput.* **2016**, *12* (3), 1331–1341.
(22) Dupont, C.; Andreussi, O.; Marzari, N. Self-Consistent Continuum Solvation (SCCS): The Case of Charged Systems. *J. Chem. Phys.* **2013**, *139* (21), 214110.
(23) Nishihara, S.; Otani, M. Hybrid Solvation Models for Bulk, Interface, and Membrane: Reference Interaction Site Methods Coupled with Density Functional Theory. *Phys. Rev. B* **2017**, *96* (11), 115429.

(24) Melander, M. M.; Kuisma, M. J.; Christensen, T. E. K.; Honkala, K. Grand-Canonical Approach to Density Functional Theory of Electrocatalytic Systems: Thermodynamics of Solid-Liquid Interfaces at Constant Ion and Electrode Potentials. *J. Chem. Phys.* **2018**, *150* (4), 041706.
(25) Sundararaman, R.; Letchworth-Weaver, K.; Schwarz, K. A. Improving Accuracy of Electrochemical Capacitance and Solvation Energetics in First-Principles Calculations. *J. Chem. Phys.* **2018**, *148* (14), 144105.
(26) Filhol, J.-S.; Neurock, M. Elucidation of the Electrochemical Activation of Water over Pd by First Principles. *Angewandte Chemie International Edition* **2006**, *45* (3), 402–406.
(27) McCrum, I. T.; Janik, M. J. PH and Alkali Cation Effects on the Pt Cyclic Voltammogram Explained Using Density Functional Theory. *J. Phys. Chem. C* **2016**, *120* (1), 457–471.
(28) Kolb, M. J.; Wermink, J.; Calle-Vallejo, F.; Juurlink, L. B. F.; Koper, M. T. M. Initial Stages of Water Solvation of Stepped Platinum Surfaces. *Phys. Chem. Chem. Phys.* **2016**, *18* (5), 3416–3422.
(29) Morais, R. F. de; Kerber, T.; Calle-Vallejo, F.; Sautet, P.; Loffreda, D. Capturing Solvation Effects at a Liquid/Nanoparticle Interface by Ab Initio Molecular Dynamics: Pt201 Immersed in Water. *Small* **2016**, *12* (38), 5312–5319.
(30) Liu, S.; White, M. G.; Liu, P. Mechanism of Oxygen Reduction Reaction on Pt(111) in Alkaline Solution: Importance of Chemisorbed Water on Surface. *J. Phys. Chem. C* **2016**, *120* (28), 15288–15298.
(31) Karlberg, G. S. Adsorption Trends for Water, Hydroxyl, Oxygen, and Hydrogen on Transition-Metal and Platinum-Skin Surfaces. *Phys. Rev. B* **2006**, *74* (15), 153414.
(32) Tripkovic, V.; Skúlason, E.; Siahrostami, S.; K. Nørskov, J.; Rossmeisl, J. The Oxygen Reduction Reaction Mechanism on Pt(111) from Density Functional Theory Calculations. *Electrochimica Acta* **2010**, *55*, 7975–7981.
(33) Gauthier, J. A.; Dickens, C. F.; Chen, L. D.; Doyle, A. D.; Nørskov, J. K. Solvation Effects for Oxygen Evolution Reaction Catalysis on IrO2(110). *J. Phys. Chem. C* **2017**, *121* (21), 11455–11463.
(34) Kamerlin, S. C. L.; Haranczyk, M.; Warshel, A. Are Mixed Explicit/Implicit Solvation Models Reliable for Studying Phosphate Hydrolysis? A Comparative Study of Continuum, Explicit and Mixed Solvation Models. *ChemPhysChem* **2009**, *10* (7), 1125–1134.
(35) Sakong, S.; Naderian, M.; Mathew, K.; Hennig, R. G.; Groß, A. Density Functional Theory Study of the Electrochemical Interface between a Pt Electrode and an Aqueous Electrolyte Using an Implicit Solvent Method. *The Journal of Chemical Physics* **2015**, *142* (23), 234107.
(36) Mills, J. N.; McCrum, I. T.; Janik, M. J. Alkali Cation Specific Adsorption onto Fcc(111) Transition Metal Electrodes. *Phys. Chem. Chem. Phys.* **2014**, *16* (27), 13699–13707.
(37) Calle-Vallejo, F.; F. de Morais, R.; Illas, F.; Loffreda, D.; Sautet, P. Affordable Estimation of Solvation Contributions to the Adsorption Energies of Oxygenates on Metal Nanoparticles. *J. Phys. Chem. C* **2019**, *123* (9), 5578–5582.

(38) Rendón-Calle, A.; Builes, S.; Calle-Vallejo, F. Substantial Improvement of Electrocatalytic Predictions by Systematic Assessment of Solvent Effects on Adsorption Energies. *Applied Catalysis B: Environmental* **2020**, 119147.
(39) Carrasco, J.; Klimeš, J.; Michaelides, A. The Role of van Der Waals Forces in Water Adsorption on Metals. *The Journal of Chemical Physics* **2013**, *138* (2), 024708.
(40) Michaelides, A.; Ranea, V. A.; de Andres, P. L.; King, D. A. General Model for Water Monomer Adsorption on Close-Packed Transition and Noble Metal Surfaces. *Phys. Rev. Lett.* **2003**, *90* (21), 216102.
(41) Michaelides, A.; Hu, P. Catalytic Water Formation on Platinum: A First-Principles Study. *J. Am. Chem. Soc.* **2001**, *123* (18), 4235–4242.
(42) Michaelides, A. Density Functional Theory Simulations of Water–Metal Interfaces: Waltzing Waters, a Novel 2D Ice Phase, and More. *Appl. Phys. A* **2006**, *85* (4), 415–425.
(43) Klimeš, J.; Bowler, D. R.; Michaelides, A. Chemical Accuracy for the van Der Waals Density Functional. *J. Phys.: Condens. Matter* **2010**, *22* (2), 022201.
(44) Greeley, J.; Mavrikakis, M. Near-Surface Alloys for Hydrogen Fuel Cell Applications. *Catalysis Today* **2006**, *111* (1), 52–58.
(45) Calle-Vallejo, F.; Koper, M. T. M.; Bandarenka, A. S. Tailoring the Catalytic Activity of Electrodes with Monolayer Amounts of Foreign Metals. *Chem. Soc. Rev.* **2013**, *42* (12), 5210–5230.
(46) Tymoczko, J.; Calle-Vallejo, F.; Schuhmann, W.; Bandarenka, A. S. Making the Hydrogen Evolution Reaction in Polymer Electrolyte Membrane Electrolysers Even Faster. *Nature Communications* **2016**, *7*, 10990.
(47) Zhao,Z.;Lu,G. Computational Screening of Near-Surface Alloys for CO2 Electroreduction. *ACS Catal.* **2018**, *8* (5), 3885–3894.
(48) Kresse, G.; Joubert, D. From Ultrasoft Pseudopotentials to the Projector Augmented-Wave Method. *Phys. Rev. B* **1999**, *59* (3), 1758–1775.
(49) Kresse, G.; Furthmüller, J. Efficient Iterative Schemes for Ab Initio Total-Energy Calculations Using a Plane-Wave Basis Set. *Phys. Rev. B* **1996**, *54* (16), 11169–11186.
(50) Methfessel, M.; Paxton, A. T. High-Precision Sampling for Brillouin-Zone Integration in Metals. *Phys. Rev. B* **1989**, *40* (6), 3616–3621.
(51) Nørskov, J. K.; Rossmeisl, J.; Logadottir, A.; Lindqvist, L.; Kitchin, J. R.; Bligaard, T.; Jónsson, H. Origin of the Overpotential for Oxygen Reduction at a Fuel-Cell Cathode. *J. Phys. Chem. B* **2004**, *108* (46), 17886–17892.
(52) Perdew, J. P.; Burke, K.; Wang, Y. Generalized Gradient Approximation for the Exchange-Correlation Hole of a Many-Electron System. *Phys. Rev. B* **1996**, *54* (23), 16533–16539.
(53) Perdew, J. P.; Burke, K.; Ernzerhof, M. Generalized Gradient Approximation Made Simple. *Phys. Rev. Lett.* **1996**, *77* (18), 3865–3868.
(54) Hammer, B.; Hansen, L. B.; Nørskov, J. K. Improved Adsorption Energetics within Density-Functional Theory Using Revised Perdew-Burke-Ernzerhof Functionals. *Phys. Rev. B* **1999**, *59* (11), 7413–7421.
(55) Grimme, S.; Antony, J.; Ehrlich, S.; Krieg, H. A Consistent and Accurate Ab Initio Parametrization of Density Functional Dispersion Correction (DFT-D) for the 94 Elements H-Pu. *J. Chem. Phys.* **2010**, *132* (15), 154104.

(56) Dion, M.; Rydberg, H.; Schröder, E.; Langreth, D. C.; Lundqvist, B. I. Van Der Waals Density Functional for General Geometries. *Phys. Rev. Lett.* **2004**, *92* (24), 246401.
(57) Wellendorff, J.; Lundgaard, K. T.; Møgelhøj, A.; Petzold, V.; Landis, D. D.; Nørskov, J. K.; Bligaard, T.; Jacobsen, K. W. Density Functionals for Surface Science: Exchange-Correlation Model Development with Bayesian Error Estimation. *Phys. Rev. B* **2012**, *85* (23), 235149.
(58) Ogasawara, H.; Brena, B.; Nordlund, D.; Nyberg, M.; Pelmenschikov, A.; Pettersson, L. G. M.; Nilsson, A. Structure and Bonding of Water on Pt(111). *Phys. Rev. Lett.* **2002**, *89* (27), 276102.
(59) Schnur, S.; Groß, A. Properties of Metal–Water Interfaces Studied from First Principles. *New J. Phys.* **2009**, *11* (12), 125003.
(60) Mattsson, A. E.; Armiento, R.; Schultz, P. A.; Mattsson, T. K. R. Nonequivalence of the Generalized Gradient Approximations PBE and PW91; 2006.
(61) Kurth, S.; Perdew, J. P.; Blaha, P. Molecular and Solid-State Tests of Density Functional Approximations: LSD, GGAs, and Meta-GGAs. *International Journal of Quantum Chemistry* **1999**, *75* (4–5), 889–909.
(62) Díaz, C.; Pijper, E.; Olsen, R. A.; Busnengo, H. F.; Auerbach, D. J.; Kroes, G. J. Chemically Accurate Simulation of a Prototypical Surface Reaction: H2 Dissociation on Cu(111). *Science* **2009**, *326* (5954), 832–834.
(63) Janthon, P.; Kozlov, S. M.; Viñes, F.; Limtrakul, J.; Illas, F. Establishing the Accuracy of Broadly Used Density Functionals in Describing Bulk Properties of Transition Metals. *J. Chem. Theory Comput.* **2013**, *9* (3), 1631–1640.
(64) Stephens, I. E. L.; Bondarenko, A. S.; Grønbjerg, U.; Rossmeisl, J.; Chorkendorff, I. Understanding the Electrocatalysis of Oxygen Reduction on Platinum and Its Alloys. *Energy Environ. Sci.* **2012**, *5* (5), 6744–6762.
(65) Calle-Vallejo, F.; Bandarenka, A. S. Enabling Generalized Coordination Numbers to Describe Strain Effects. *ChemSusChem* **2018**, *11* (11), 1824–1828.
(66) Calle-Vallejo, F.; Martínez, J. I.; García-Lastra, J. M.; Rossmeisl, J.; Koper, M. T. M. Physical and Chemical Nature of the Scaling Relations between Adsorption Energies of Atoms on Metal Surfaces. *Phys. Rev. Lett.* **2012**, *108* (11), 116103.
(67) Calle-Vallejo, F.; Inoglu, N. G.; Su, H.-Y.; Martínez, J. I.; Man, I. C.; Koper, M. T. M.; Kitchin, J. R.; Rossmeisl, J. Number of Outer Electrons as Descriptor for Adsorption Processes on Transition Metals and Their Oxides. *Chem. Sci.* **2013**, *4* (3), 1245–1249.
(68) Su, H.-Y.; Sun, K.; Wang, W.-Q.; Zeng, Z.; Calle-Vallejo, F.; Li, W.-X. Establishing and Understanding Adsorption–Energy Scaling Relations with Negative Slopes. *J. Phys. Chem. Lett.* **2016**, *7* (24), 5302–5306.